Korean J. Chem. Eng., 40(9), 2174-2186 (2023)
DOI: 10.1007/s11814-023-1459-2

pISSN: 0256-1115
eISSN: 1975-7220

Hydrogen production by catalytic steam reforming of waste cooking oil over La-Ni/ZSM-5 catalyst

Na Xiao, Rui Zhao, Yufei Liu, Wei Zhan, Yonghui Xu, and Zhengshun Wu†

Chemistry College, Central China of Normal University, Wuhan 430079, China
(*Received 11 October 2022 • Revised 13 March 2023 • Accepted 25 March 2023*)

Abstract−Ni/ZSM-5 catalyst is one of the promising catalysts to improve the catalytic steam reforming of waste cooking oil (WCO) for hydrogen production. Furthermore, the introduction of lanthanum (La) plays a huge role in inhibiting metal sintering and carbon deposition and improving the stability and activity of the catalyst. This study investigated the effects of reaction temperature (600-800 °C), steam to carbon molar ratio (S/C), n Ni/ZSM-5 (n=5, 10, and 15 wt%), and the addition of promoter (La) on the experimentally generated hydrogen yield and carbon deposition. Results showed that the experiment used 6 wt% La-10 wt% Ni/ZSM-5 at 0.1 MPa, 700 °C, space-time (τ)=0.56 $g_{catalyst}h/g_{WCO}$, and S/C=5.25, which obtained the yield of H_2 was 154.12 mol/kg, carbon deposition was 5.38%. Therefore, Ni-modified catalyst added La to improve the catalyst coking resistance and prevent carbon formation. Moreover, La can further promote the dispersion of nickel on the surface of the carrier and improve the catalytic performance of the catalyst for steam reforming reaction.

Keywords: Waste Cooking Oil, Catalytic Steam Reforming, Hydrogen Production, La Promoter, Carbon Deposition

INTRODUCTION

Most of the chemical and physical properties of waste cooking oil (WCO) are attributed to their fatty acid composition, which makes its composition different from that of general crude oils [1]. Generally, as an environmental pollutant, WCO is discharged through the public sewage system, which can seriously pollute the water and atmosphere. Some illegal traders even process it into gutter oil and re-enter the market, which endangers people's health. WCO improperly used can even cause disease [2,3]. The redevelopment of WCO is changed from hazardous waste to valuable raw materials for industrial applications. First, the use and treatment of WCO could significantly reduce the cost of water treatment caused by discharging it directly into the sewer. Secondly, WCO can be used as the primary raw material in many industrial processes without special treatment. In addition, WCO has shown great potential as a hydrogen supplier.

Hydrogen is an ideal clean, high-energy fuel, and energy carrier with considerable potential in the future global economy [4]. Hydrogen is used widely in chemical, fertilizer, food, and metallurgical industries as an essential raw material chemical [5]. Most hydrogen is produced on an industrial scale from heavy oil fractions by catalytic steam reforming fossil fuels such as natural gas, coal, and naphtha. Since carbon dioxide is produced in large amounts during the production of hydrogen by steam reforming hydrocarbons, its utilization can cause environmental degradation if the consumption of fossil fuel resources must meet the demand for hydrogen. Therefore, hydrogen can be obtained from clean and renewable energy sources, which can realize the true potential of hydrogen energy systems [6]. Hydrogen production from steam reforming of WCO can be improved by adding Ni-modified catalysts. However, the carbon deposition problem is severe. Therefore, it can be achieved by the introduction of lanthanum (La).

The steam reforming process is viable for producing renewable energy [7]. The carbon deposits generated by the cracking of WCO will block the active center of the catalyst, which can reduce the catalyst's reactivity and the production of H_2. Therefore, steam reforming is used to reduce the carbon deposition produced by the experiment. In the steam reforming reaction, the organic molecule ($C_nH_mO_k$) is converted into carbon monoxide and hydrogen according to reaction (1). Carbon monoxide and hydrogen then react to form methane and carbon dioxide through the equilibrium reactions (2) and (3). Thus, the gas mixture composition at the reactor outlet almost reachesa equilibrium [8]. The main reactions are as follows:

$$C_nH_mO_k+(n-k)H_2O\leftrightarrow nCO+(n+m/2-k)H_2 \quad (1)$$

$$CO+H_2O\leftrightarrow H_2+CO_2 \quad (2)$$

$$3H_2+CO\leftrightarrow CH_4+H_2O \quad (3)$$

Then complete steam reforming is described by the following reaction:

$$C_nH_mO_k+(2n-k)H_2O\leftrightarrow nCO_2+[2n+m/2-k]H_2 \quad (4)$$

Ni has been extensively used as an active metal for steam reforming oxygenates due to its high activity for C-C bond rupture and H_2 formation from H atoms [9,10]. Chen et al. [11] researched steam reforming of bio-oil with an emphasis on catalyst development. They found that the nickel-loaded catalyst has high reactivity in C-C and C-H bond cleavage. Yan et al. [12] used Ni/ZSM-5

†To whom correspondence should be addressed.
E-mail: wuzs@ccnu.edu.cn

catalyst for the aqueous reforming of phenol. The results showed that the Ni/ZSM-5 catalyst with Ni content of 16 wt% and Si/Al molar ratio of 25 had better catalytic performance. Awadallah et al. [13] used Ni-Mo/Al_2O_3 as a catalyst for the direct decomposition of methane. When the Ni content was 40% and the Mo content was 6.5%, the maximum hydrogen yield was about 90%. Gutta et al. [14] investigated the effect of loaded Ni (10-50 wt%) on MCM-41 and found that 50 wt% Ni/MCM-41 exhibited higher hydrogen yield and lifetime. However, nickel-based catalysts are thermodynamically liable to active site sinter and carbon deposition [15]. Therefore, catalysts introduced La to adjust the acidity and improved the anti-carbon deposition ability of the catalysts, which effectively enhanced the catalytic activity and stability [16-18].

The introduction of lanthanum into the catalyst can not only improve the catalytic activity of the catalyst, but also effectively reduce carbon deposition. Adamu et al. [19] and Chowdhury et al. [20] investigated the effect of La modified Ni/Al_2O_3 catalyst on glucose SCWG, and their results showed that the catalyst exhibited good performance in enhancing H_2 production. Boudjeloud et al. [21] found that La-added in Ni/Al_2O_3 promoted the formation of the Ni-La-Al structure and caused highly dispersed nickel particles, which enhanced the dissociative adsorption of CHx species. Lu et al. [22] studied that after loading a small content of metal elements such as Fe and La on Ni-based catalysts, adding La will promote the dispersion of NiO nanoparticles. The carbon deposition produced during the experiment has been the reason for affecting the catalytic activity of the catalyst. Since reactions (5) and (6) occurred, La_2O_3 will react with CO_2 to form like $La_2O_2CO_3$ and then interact with carbon deposits (C) to release CO and regenerate La_2O_3, which controls the carbon accumulation rate and reduces carbon deposition [17,23-26].

$$La_2O_3+CO_2 \leftrightarrow La_2O_2CO_3 \quad (5)$$

$$La_2O_2CO_3+C \leftrightarrow La_2O_3+CO \quad (6)$$

Although there is much research on supported La catalysts, little research has used the La-loaded catalyst to produce hydrogen in the experiment of catalytic steam reforming of WCO. This paper studied the effects of temperature (600-800 °C), steam to carbon molar ratio (S/C=0.64-10.95), H-ZSM-5, nickel-loaded (n Ni/ZSM-5 (n=5, 10, and 15 wt%)) and the introduction of La on hydrogen production from cracking of WCO to enhance H_2 yield and reduced carbon deposits.

Table 1. The elemental analysis of WCO

Elemental analysis (wt%)				
Sample	Carbon	Hydrogen	Oxygen	Nitrogen
1	75.99	10.02	13.2	0.79
2	76.62	9.73	12.8	0.85
3	75.37	9.64	14.3	0.69
Standard deviation	0.63	0.20	0.78	0.08

EXPERIMENTAL SECTION

1. Materials and Catalyst Preparation

The experimental raw materials were mainly from waste oil after fried food in local restaurants in Wuhan. The H-ZSM-5 used in the experiment was produced by Zoran Environmental Protection Technology (Dalian) Co., Ltd, with a silicon-aluminum ratio of 45 and a white spherical shape. Nickel nitrate ($Ni(NO_3)_2 \cdot 6H_2O$) was purchased from Shanghai Wo Biotechnology Co., Ltd., and lanthanum nitrate ($La(NO_3)_3 \cdot 6H_2O$) was purchased from Wuhan Yiruisi Technology Co., Ltd. The elemental analysis results of WCO are shown in Table 1. From the elemental analysis of WCO, the chemical formula of WCO was determined to be $CH_{1.58}O_{0.14}N_{0.009}$.

We used H-ZSM-5 as the carrier to prepare the n Ni/ZSM-5 (n=5, 10, and 15 wt%) and 6 wt% La-10 wt% Ni/ZSM-5 by the impregnation method. In a typical synthesis, taking 5 wt% Ni/ZSM-5 catalyst as an example, 1.24 g of nickel nitrate hexahydrate $Ni(NO_3)_2 \cdot 6H_2O$ was dissolved in excess deionized water to make a nickel nitrate solution. 5 g of H-ZSM-5 was weighed and mixed with nickel nitrate solution, placed in ultrasonic reaction for 4 hours,

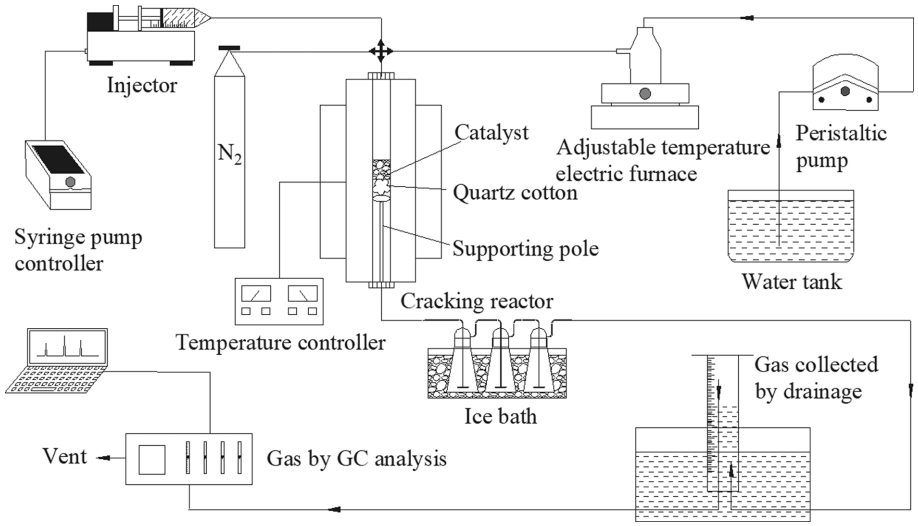

Fig. 1. Diagram of the experimental system.

and then dried in an oven at 105 °C for 12 hours. The dried samples were calcined in a muffle furnace at 550 °C for 4 hours. Then, the catalyst was reduced to a metal state by passing H_2 into it at 600 °C. The above method prepared the 10 wt% Ni/ZSM-5, 15 wt% Ni/ZSM-5, and 6 wt% La-10 wt% Ni/ZSM-5 catalysts.

2. Reaction Equipment and Operating Conditions

The experimental equipment is shown in Fig. 1. The injection device adopted was the model TJ-3A syringe pump produced by Baoding Lange Constant Current Pump Co., Ltd. to complete the injection of WCO. The model of the adjustable closed electric furnace in the device used in the gasification chamber is FL-1, which was produced by Beijing Yongguang Medical Equipment Factory. The water flow regulated device was a peristaltic pump of model YZ1515X produced by Baoding Lange Constant Current Pump Co., Ltd.

Before the start of the experiment, the catalyst was loaded into the fixed-bed reactor (inner diameter: 20 mm; outer diameter: 25 mm). The reactor was purged with nitrogen at a flow rate of 50 mL/min, which kept the reactor under an inert atmosphere. Then, the WCO was injected into the reactor through a syringe pump, and steam was introduced simultaneously. After 30 min of reaction, the outlet gas was collected and analyzed by GC. The experiments were carried out under the following conditions:

(a) The effect of temperature (600-800 °C) on hydrogen production from cracking of WCO was investigated under the condition of 0.1 MPa.
(b) The effect of steam-to-carbon molar ratio (S/C) is 0.64-10.95 on hydrogen production from steam reforming of WCO was studied under the conditions of 0.1 MPa and 700 °C.
(c) The effect of S/C (0.64-10.95) on hydrogen production from catalytic steam reforming of WCO was investigated under the conditions of 0.1 MPa, 700 °C, space-time (τ)=0.56 $g_{catalyst}h/g_{WCO}$, and added H-ZSM-5.
(d) The effects of the addition of n Ni/ZSM-5 (n=5, 10, and 15 wt%) on hydrogen production from catalytic steam reforming of WCO were investigated under the conditions of 0.1 MPa, 700 °C, space-time (τ)=0.56 $g_{catalyst}h/g_{WCO}$, and S/C=5.25.
(e) The effects of temperature (600-800 °C) on hydrogen production from catalytic steam reforming of WCO were studied under the conditions of 0.1 MPa, space-time (τ)=0.56 $g_{catalyst}h/g_{WCO}$, S/C=5.25, and added 6 wt% La-10 wt% Ni/ZSM-5.

The gas yield of hydrogen was calculated according to Eq. (7):

$$Y_{H_2}(\text{mol/kg}) = \frac{P_{H_2}(\text{mol})}{M_{WCO}(\text{kg})} \quad (7)$$

where, Y_{H_2} is the yield of H_2, and P_{H_2} is moles of production H_2, and is mass of WCO.

The steam-to-carbon molar ratio (S/C) was calculated according to Eq. (8):

$$S/C = \left(\frac{m_s}{m_{WCO}}\right) / \left(\frac{m_s}{m_{WCO}}\right)_{st} = \frac{m_s(\text{mol})}{1.86 \times (m_{WCO})(\text{mol})} \quad (8)$$

where, m_s refers to the moles of steam, and m_{WCO} refers to the moles of WCO, and st refers to the stoichiometry.

3. Analytical Techniques

Inductively coupled plasma emission spectrometry (ICP-OES) was used to determine the actual load of nickel on the catalyst. The model of the instrument used for analysis is the Agilent ICPOES730. Approximately 0.01-0.038 g of the sample was removed, homogenized and placed into a hot block tube. Trace metal-grade hydrochloric (0.75 ml) and nitric (2.25 ml) acids were added to each tube, placed in the hot block, and refluxed for 3 h at 95 °C. The samples were cooled and brought to the final volume of 25 ml with DI water. All samples were analyzed at 50× dilution due to the very high levels of the target elements. Standard quality assurance procedures were employed, including analyzing initial and continuing calibration checks and blanks, duplicate samples, preparation blanks (Blank), postdigestion spiked samples, and laboratory control samples (LCS).

XRD was used to observe carbon residue and crystal form changed after loading metal. The X-ray diffractometer (XRD) used in this experiment was produced by Bruker, Germany, model Bruker D8 Advance. XRD operated at 45 kV and 40 mA via the Cu Kα radiation, and the diffraction (2θ) was carried out in the range from 5° to 80° with a scan rate of 10°/min.

Electron microscopy (SEM) was performed to visualize the morphology of the catalyst. A minute quantity sample was taken directly to the conductive adhesive and used the Oxford Quorum SC7620 sputter coater to spray gold for 45 s, and the gold spray was 10 mA. Then, the sample morphology was photographed using a Zeiss Gemini SEM 300 scanned electron microscope produced by Carl Zeiss, Germany, under an accelerated voltage of 3 kV.

The O_2-TPO experiments were executed in order to find the nature and/or type of coke deposits over spent catalysts. The experiment was conducted on an AutoChem1 II 2920 apparatus manufactured by Micromeritics. In a U-type tube loaded with 50-100 mg sample and dried and pretreated by increasing the temperature from room temperature to 300 °C at a rate of 10 °C/min. And then, the samples were purged for 1 hour under a He atmosphere (30-50 ml/min) to remove moisture from the models. After cooling to 50 °C, the samples were bubbled into a 10% O_2-He gas mixture (30-50 ml/min) for 1 hour to adsorb O_2 to saturation. After saturation, the residual O_2 was purged at 30-50 ml/min for 1 hour in a He flow until the outlet gas could not detect O_2. Finally, the temperature of the samples was raised to 600 °C at a heating rate of 10 °C/min under a He atmosphere for NH_3 adsorption measurement, and a thermal conductivity detector (TCD) detected the desorbed gas.

The strength and number of acid sites in the catalyst were analyzed by temperature-programmed desorption of NH_3-TPD on an AutoChem1 II 2920 apparatus manufactured by Micromeritics. The method is the same as TPO, except that the gas mixture used is the NH_3-He gas mixture.

The studies of the mixture of WCO and catalyst were carried out through Py-GC/MS technique to analyze the pyrolytic vapor. Pyrolysis experiments were performed through Multi-Shot Pyrolyzer EGA/PY-3030D pyrolyzer. The pyrolyzer was combined with a Clarus 560 GC/MS instrument produced by PerkinElmer, USA. The pyrolysis products were chromatographically separated on an HP-5MS elastic quartz capillary column (30 m×0.25 mm i.d., 0.25 mm film thickness). In this study, Py-GC/MS was carried out in a single shot analysis mode at 700 °C. Helium (99.999%) as a carrier gas, which was used at a constant flow rate of 1.5 ml/min with a split ratio of

1 : 80. The initial temperature was set at 200 °C with a heating rate of 6 °C/ min and then 250 °C by employing a higher heating rate of 15 °C/min. WCO and catalyst were mixed at 1 : 1, and approximately 1 mg of the sample was taken for each test. Each experiment was repeated three times to ensure reproducibility.

Furthermore, the relative abundance ($R_{abundance}$) of pyrolytic products and the selectivity of aromatics ($S_{aromatics}$) are calculated as [27]:

$$R_{abundance} = \frac{P_i}{P_{total}} \quad (9)$$

where, P_i is the peak area of certain identified product, and P_{total} is the total peak area under certain condition.

A gas chromatograph (GC), model GC-9280, produced by Beijing Purui Analytical Instrument Co., Ltd, was used to analyze the volume fraction of gas produced by the experiment of catalytic steam reforming of WCO. The instrument maintained the column temperature at 120 °C, used high-purity Argon as the carrier gas, adopted a molecular sieve chromatographic column, and the detector TCD was the thermal conductivity detector. The device could detect CO, CH_4, H_2, and CO_2. The experiment was repeated three times and then calculated the average value of the volume content of the four gas components (H_2, CH_4, CO, CO_2).

RESULTS AND DISCUSSION

1. Characterization of Catalysts

1-1. ICP-OES Analysis

Table 2 shows the ICP-OES results of the actual Ni and La loading on the catalyst. The results indicate that Ni and La were successfully impregnated in the catalyst, and the actual loading rate was

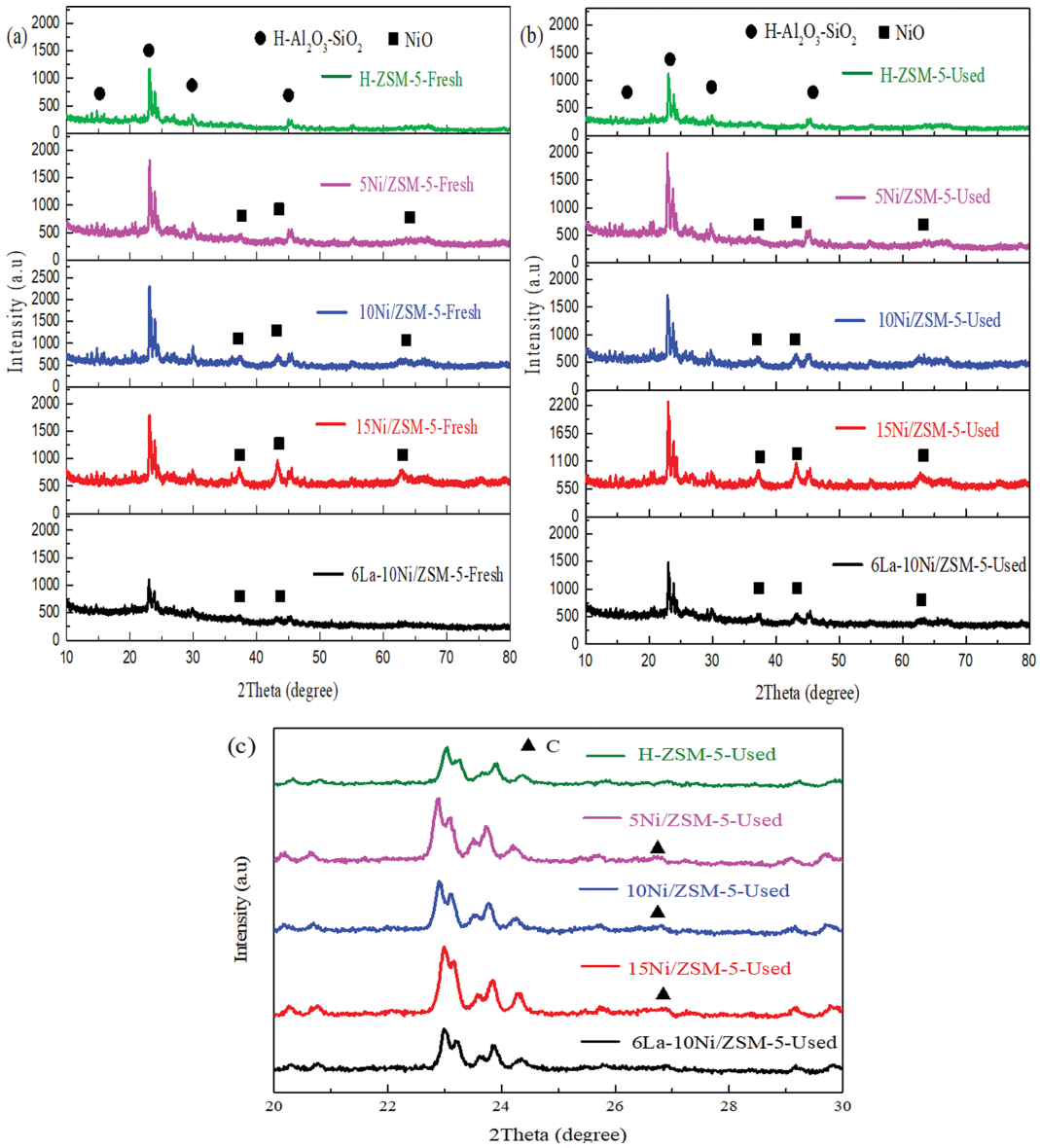

Fig. 2. XRD patterns of H-ZSM-5, 10 wt% Ni/ZSM-5, and 6 wt% La-10 wt% Ni/ZSM-5: (a) Fresh catalysts; (b) The catalysts after-use; (c) The catalysts after-use (20-30°).

Table 2. Ni and La loading percentage of catalysts used in this study

Sample	Ni concentration		La concentration	
	Measured by ICP-OES (wt%)	Theoretical value (wt%)	Measured by ICP-OES (wt%)	Theoretical value (wt%)
5 wt% Ni/ZSM-5	4.39	5	-	-
10 wt% Ni/ZSM-5	10.11	10	-	-
15 wt% Ni/ZSM-5	14.94	15	-	-
6 wt% La-10 wt% Ni/ZSM-5	10.14	10	6.28	6

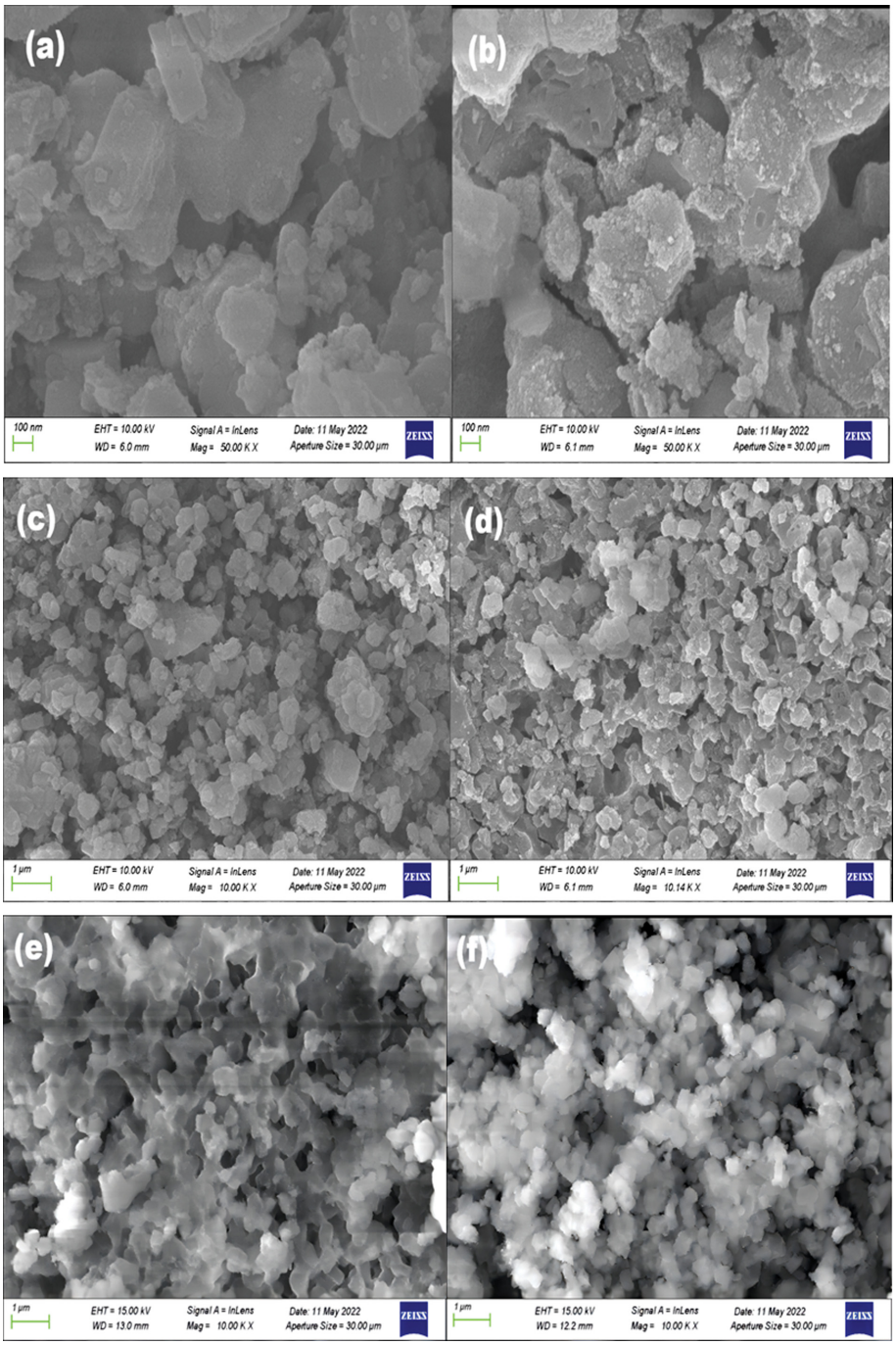

Fig. 3. SEM images of (a) Fresh H-ZSM-5, (b) Used H-ZSM-5, (c) Fresh 10 wt% Ni/ZSM-5, (d) Used 10 wt% Ni/ZSM-5, (e) Fresh 6 wt% La-10 wt% Ni/ZSM-5, and (f) Used 6 wt% La-10 wt% Ni/ZSM-5.

close to the theoretical value.

1-2. XRD Analysis

The X-ray diffraction patterns of the fresh and after-used catalysts are shown in Fig. 2(a) and (b). All catalysts exhibited characteristic peaks of H-ZSM-5 at angles (2θ) of 14.6°, 23.4°, and 45.2° (PDF card #38-195). The characteristic peak of the H-ZSM-5 molecular sieve remained after an addition of different content of Ni on the H-ZSM-5 carrier, indicating that its structure was not damaged during metal impregnation treatment [28]. This phenomenon indicates that H-ZSM-5 has commendable stability to maintain its crystal structure unchanged after the metal is loaded or the addition to promoter and calcination process [26,29,30]. The catalyst of Ni-modified ZSM-5 showed the NiO phase peaks exhibited at degrees (2θ) of 37.3°, 43.3°, and 62.9° (PDF card #47-1049) [31].

The characteristic diffraction peaks of La_2O_3 phases were not detected after in addition to 6 wt% La on 10 wt% Ni/ZSM-5 catalyst. The possible reasons were the La_2O_3 was highly dispersed on the surface of the 10 wt% Ni/ZSM-5 catalyst or formed the micromorphological grain below the XRD's detection limit [32-34]. Note that all strengths of the peaks corresponding to the 6 wt% La-10 wt% Ni/ZSM-5 have a decreasing tendency compared with all Ni-loaded catalysts. This phenomenon illustrates that the molecular sieve interacted with the nickel species and the promoter [35,36]. It also means that the La-added could further form more active centers, which improves the catalytic performance of the catalyst for steam reforming reaction [37].

It can be seen from Fig. 2(c) that after the catalysts, a characteristic peak of carbon was detected at a degree (2θ) of 26.66° (PDF card # 26-1077). The carbon peak in 6 wt% La-10 wt% Ni/ZSM-5 was not apparent, which indicated that it did not produce carbon or formed the micromorphological grain below the XRD's detection limit.

1-3. SEM Analysis

The SEM images in Fig. 3 depict the morphology of the fresh and after-use H-ZSM-5, 10 wt% Ni/ZSM-5, and 6 wt% La-10 wt% Ni/ZSM-5 catalysts. In Fig. 3(a), the H-ZSM-5 presents dispersed particles, from which one can observe that the crystalline grains grow into cubic shapes. H-ZSM-5, 10 wt% Ni/ZSM-5, and 6 wt% La-10 wt% Ni/ZSM-5 have similar morphologies. The loaded Ni and La via the impregnation method did not change zeolite morphology [38]. As shown in Fig. 3(b), the particle size of H-ZSM-5 slightly increased after participating in the catalytic steam reforming experiment of WCO. The surface became rough in the H-ZSM-5, and the fragmented substances can be seen. These fragments may be carbon generated during the reaction. In Fig. 3(c), it can be observed that the 10 wt% Ni/ZSM-5 catalyst has a uniform morphology, the surface is more compacted, and the gap is smaller than H-ZSM-5. It is attributed to grain size with surface Gibbs free energy and catalyst power appearing in the aggregation due to the interconnection, which covers the catalyst surface [39,40]. In Fig. 3(e), the degree of aggregation of La-loaded catalyst particles is small because the La_2O_3 improved the electronic state of Ni or modified an appropriate interaction of NiO-La_2O_3 and Ni-ZSM-5. Hence, La_2O_3 was vital in suppressing particle aggregation [41,42]. However, the disadvantage of using SEM in this experiment is that there is no apparent carbon deposit on the surface of the used catalyst.

1-4. O_2-TPO Analysis

Normally, several types of carbon deposition can occur over Ni-based catalysts, for instance atomic carbon, amorphous carbon and graphitic carbon. These carbons can be gasified to CO and/or CO_2, under an oxidative atmosphere, at different temperatures: atomic carbon (C_α)<250 °C, amorphous carbon (C_β) 250-600 °C and graphitic carbon (C_γ)> 600 °C). The first two types are active as compared to graphitic; moreover, atomic and amorphous carbon has slower deactivation rate while graphitic, being more inactive, has a rapid deactivation rate [43]. In Fig. 4 is the TPO diagram of the spent catalyst in the catalytic steam reforming experiment of WCO at 700 °C. It can be seen that amorphous carbon deposition was detected at 500-600 °C for all catalysts. The TPO curve of the used 6 wt% La-10 wt% Ni/ZSM-5 catalyst had less carbon deposition at 500-600 °C than that of other used catalysts, which indicated that its coking resistance was strong. This aligns with its better and more stable performance in the experimental hydrogen production process by catalytic steam reforming of WCO. This shows that the

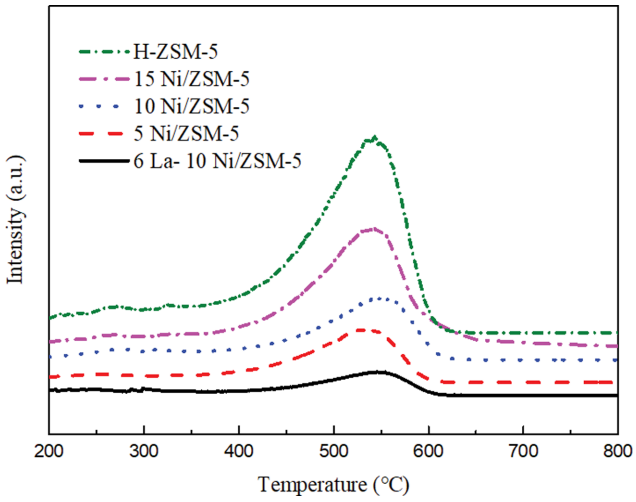

Fig. 4. O_2-TPO curve of after-used catalysts.

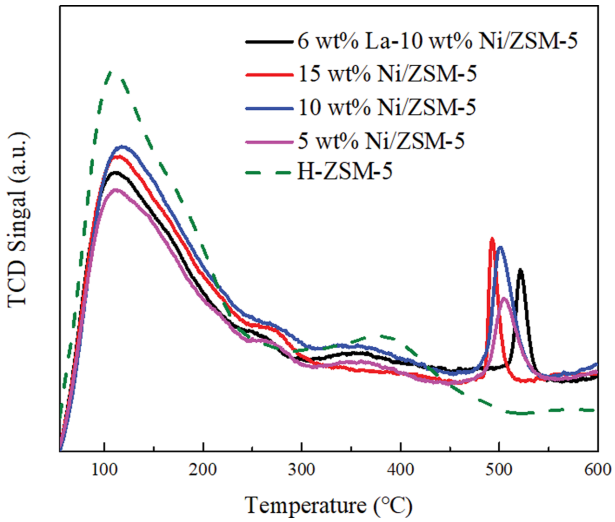

Fig. 5. NH_3-TPD profiles of the H-ZSM-5, n Ni/ZSM-5 (n=5, 10, and 15 wt%), and 6 wt% La-10 wt% Ni/ZSM-5.

Table 3. The acidity of H-ZSM-5, n Ni/ZSM-5 (n=5, 10, and 15 wt%), and 6 wt% La-10 wt% Ni/ZSM-5

Catalysts	Temperature at maximum (°C)		Quantity (mmol/g)		Peak concentration (%)	
	Weak	Strong	Weak	Strong	Weak	Strong
H-ZSM-5	115.2	377.9	3.78434	0.69542	1.32723	0.47792
5 wt% Ni/ZSM-5	110.0	505.0	4.00579	0.96629	0.92166	0.56356
10 wt% Ni/ZSM-5	117.8	500.7	4.24661	0.75997	1.06647	0.73431
15 wt% Ni/ZSM-5	115.4	492.3	4.30895	0.76532	1.03173	0.76185
6 wt% La-10 wt% Ni/ZSM-5	110.5	521.6	3.91500	1.02297	0.98386	0.66095

introduction of lanthanum into nickel-based catalysts can activate the oxidation of carbon species, and the interaction between carbon and nickel particles will affect the oxidation temperature of carbon species.

1-5. NH_3-TPD Analysis

In Fig. 5, the NH_3-TPD spectrum has two NH_3 desorption peak ranges, located at low temperature (100-240 °C) and high temperature (330-550 °C), referred to as weak and strong acid sites, respectively [44,45]. Compared with H-ZSM-5, in all Ni-modified ZSM-5 and adding La to the catalyst, the formation of the strong acid peak was pronounced at about 500 °C. Moreover, the peak position of the weak and strong acid sites shifted to a higher temperature [31]. In general, the higher the temperature at the peak position, the stronger the acid site of the catalyst. It is worth noting that the increase of acid strength on all Ni-modified ZSM-5 was due to the protonation of H+ ions (reaction (10)) after the reduction of NiO to form vital conjugated acid species, nickel sites. Previous studies have shown that Lewis and Brønsted acid sites help increase the catalyst's cracking capacity, which reduces the isomerization reaction [46,47].

$$Ni^{2+}+H_2=Ni+2H^+ \quad (10)$$

The catalyst of adding lanthanum compared with the Ni-modified ZSM-5 showed no apparent migration phenomenon of the weak acid sites, which were still at about 108 °C. This phenomenon indicated that the lanthanum introduction does not considerably change the strength of weakly acidic sites [48]. However, the strongly acidic sites shifted to a higher temperature, which reflected that loaded La significantly affected the surface acid type of the 10 wt% Ni/ZSM-5 catalyst and the number of surface acid sites. Loading the lanthanum on the 10 wt% Ni/ZSM-5 changed the acid amounts of the catalyst: with the addition of lanthanum, the acid amounts of the strongly acidic sites of the 10 wt% Ni/ZSM-5 catalyst increased from 0.75997 to 1.02297 mmol/g [30,49,50]. The acid amounts of the catalyst are shown in Table 3.

2. PY-GC/MS Analysis and the Possible Reaction Pathways

2-1. PY-GC/MS Analysis

Fig. 6(a) and (b) depict the relative abundance and the aromatics selectivity (%) of the products from catalytic cracking of WCO by the H-ZSM-5, n Ni/ZSM-5 (n=5, 10, and 15 wt%), and 6 wt% La-10 wt% Ni/ZSM-5. After La loading, the relative abundance of olefins increases significantly to 96.92%. With the increase in nickel loading, the relative abundance of olefins shows an increasing trend, which is 84.51%, 90.99%, and 93.84% for 5 wt% Ni-ZSM-5, 10 wt% Ni-ZSM-5, and 15 wt% Ni-ZSM-5, respectively. The main products of olefins are propylene and butylene, so they could be regarded as the signal for the catalytic cracking of WCO. With the addition of nickel and lanthanum, the intensity of the peak decreases gradually, which indicates that the addition of metal could promote the cracking of WCO. The relative abundance of aromatics in H-ZSM-5 is 16.4%. The deoxygenated products, which perform as hydrocarbon precursors, can get access to the acidic sites in micropores of H-ZSM-5. The deoxygenated products, which perform as hydro-

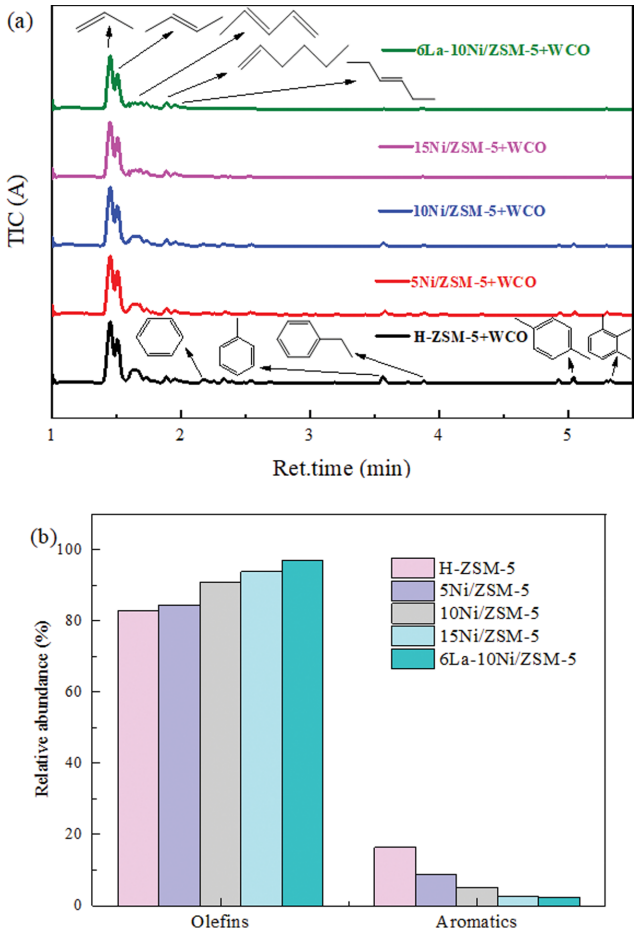

Fig. 6. The PY-GC/MS analysis and relative abundance from catalytic cracking of WCO by the H-ZSM-5, n Ni/ZSM-5 (n=5, 10, and 15 wt%), and 6 wt% La-10 wt% Ni/ZSM-5: (a) The PY-GC/MS analysis; (b) The relative abundance of the products.

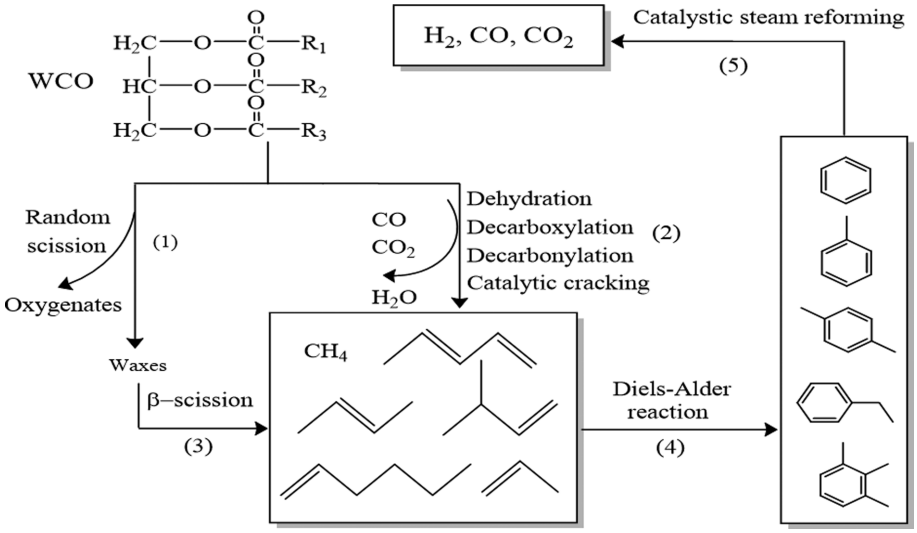

Fig. 7. The possible reaction mechanism.

Table 4. Experimental conditions for cracking WCO

Experimental condition			
Temperature (°C)	600-800	Space-time (τ) ($g_{catalyst}h/g_{WCO}$)	0
S/C	0	Filling height (cm)	8
Pressure (MPa)	0.1	Reaction time (min)	30

carbon precursors, can get access to the acidic sites in micropores of H-ZSM-5 [51,52].

In this paper, PY-GC/MS analysis provides a theoretical basis for the research on the experiments of catalytic cracking of WCO and the possible reaction mechanism. In the PY-GC/MS analysis results, it can be found that the products after pyrolysis of WCO contained aromatics and olefins. After the steam was introduced in the experiment, olefins could react with water to form alcohols in the presence of the catalyst. The aromatics and alcohols could be converted into H_2, CO, and CO_2 due to the steam reforming reaction.

2-2. The Possible Reaction Pathways

In Fig. 7, the WCO is partly converted to waxes and oxygenates through random scission during the thermal conversion process (1). Catalytic cracking of long-chain hydrocarbons into small molecules by catalyst is associated with hydrogen transfer, β-scission, and termination [53]. The acidic sites of the catalysts could abstract hydrogen atoms from aliphatic hydrocarbons to generate carbanions, which are unstable and prone to β-scission to form short olefins (3). WCO can be directly decomposed into hydrocarbons through decarboxylation to release CO_2 or decomposed into long-chain aldehydes and ketenes because the catalysts can provide acidic protons (H^+) (2). The cracking of ketenes and partial alkenals will produce small hydrocarbon molecules, which include CH_4 and short-chain hydrocarbons [54]. In other words, they are converted into hydrocarbons by releasing CO through a decarbonylation reaction. At the same time, decarboxylation, dehydration and other reactions would also generate CO_2 and H_2O. Aromatic hydrocarbons were formed by the Diels-Alder reaction (4) [55,56]. Finally, aromatics would be converted into H_2, CO, and CO_2 through steam reforming reaction (5). Steam reforming of benzene and toluene can be carried out by steam reforming reactions (Reactions (11)-(14)). In addition, the water-gas shift reaction (Reaction (2)) may occur and affect the distributions of the product. Xu et al. [57] believed that both the steam reforming reaction (Reactions (11)-(14)) and the water-gas shift reaction (Reaction (2)) occurred in parallel [58,59].

Steam reforming of toluene:

$$C_6H_5-CH_3+7H_2O\rightarrow 7CO+11H_2 \quad (11)$$

$$C_6H_5-CH_3+14H_2O\rightarrow 7CO_2+18H_2 \quad (12)$$

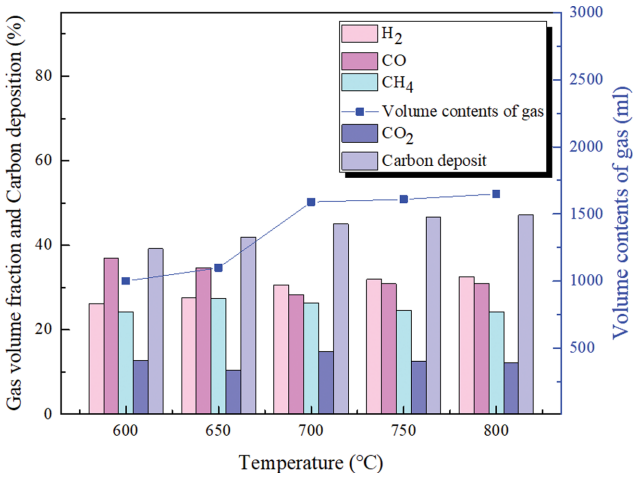

Fig. 8. Effects of the volume fraction of gas, carbon deposition rate, and volume content of gas (600-800 °C).

Table 5. Experimental conditions with or without H-ZSM-5 in WCO catalytic cracking experiment

Experimental condition			
Catalyst	H-ZSM-5	Space-time (τ) ($g_{catalyst}h/g_{WCO}$)	0.56
Temperature (°C)	700	Filling height (cm)	8
S/C	0.64-10.95	Reaction time (min)	30
Pressure (MPa)	0.1		

Steam reforming of benzene:

$$C_6H_6+6H_2O\rightarrow 6CO+9H_2 \quad (13)$$

$$C_6H_6+12H_2O\rightarrow 6CO_2+15H_2 \quad (14)$$

3. The Experiment of Hydrogen Production by Catalytic Steam Reforming of WCO

3-1. Influence of Temperature

The experimental conditions are shown in Table 4.

Fig. 8 shows that with the temperature changed, the volume content of gas by cracking of WCO would also change to a certain extent. The volume fraction of CH_4 and CO_2 decreased with the temperature increase, while H_2 increased. After 700 °C, the reaction system remained in equilibrium. It can be seen that the increase in temperature was beneficial to the preparation of H_2.

3-2. Influence of the Addition of H-ZSM-5

The experimental conditions are shown in Table 5.

This experiment set the gasification temperature at 700 °C and the pressure at 0.1 MPa. Fig. 9(a) represents that with the increase of S/C, the volume fraction of CH_4 and CO gradually decreased, while CO_2 and H_2 increased. Among them, the volume fraction of H_2 reached the commanding height after S/C=5.25, and then the volume fraction of H_2 remained unchanged.

Fig. 9(b) represents that after H-ZSM-5 adding to the experi-

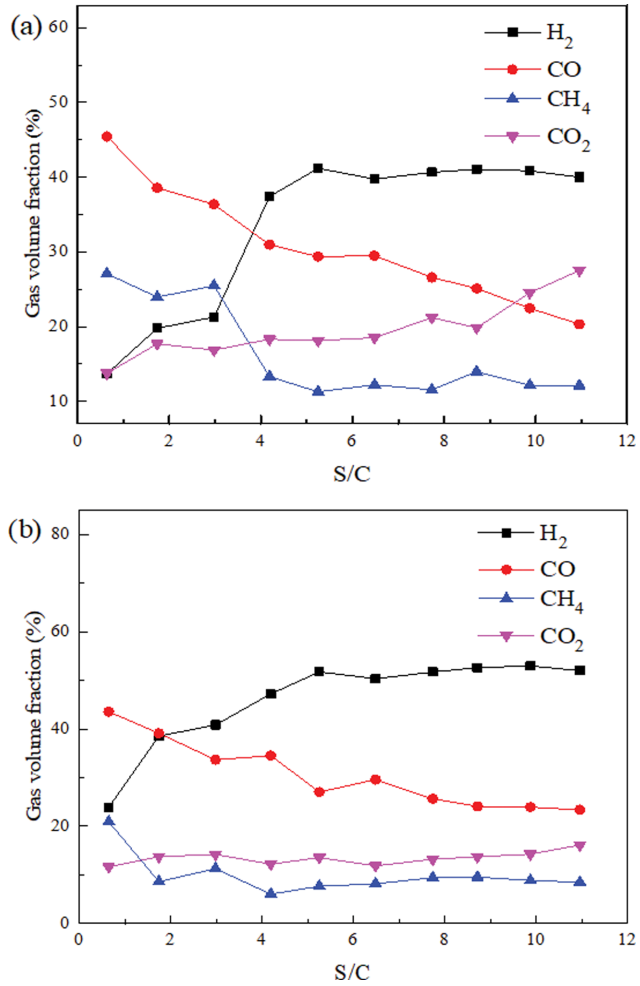

Fig. 9. Effects of S/C on gas volume fraction in the catalytic cracking experiment of WCO with or without H-ZSM-5: (a) Without H-ZSM-5; (b) Adding H-ZSM-5.

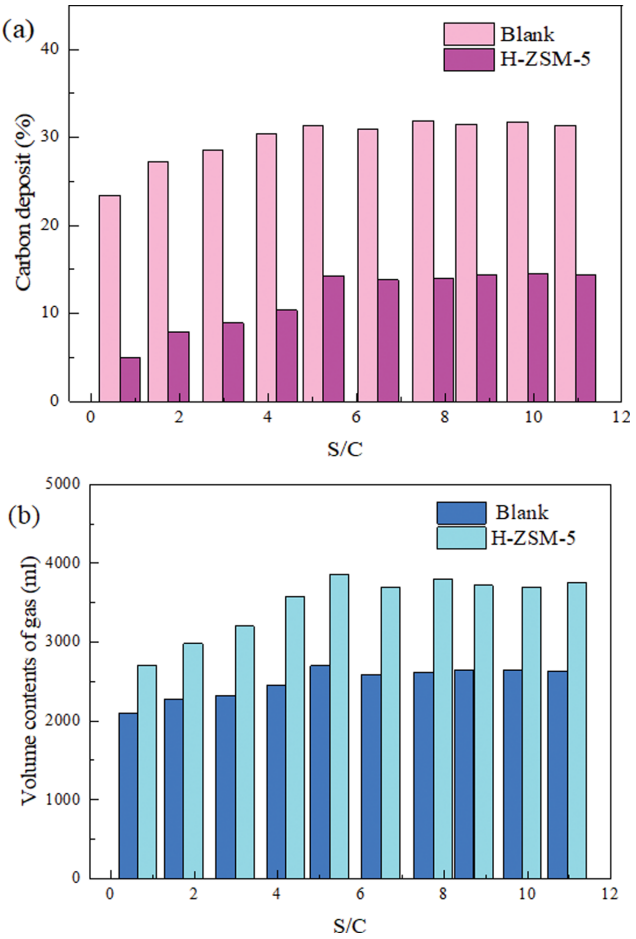

Fig. 10. Effects of S/C and H-ZSM-5 on the carbon deposition and volume contents of gas: (a) The effect of carbon deposition; (b) The effect of the volume contents of gas.

Table 6. Experimental conditions using n Ni/ZSM-5 (n=5, 10, and 15 wt%) in the experiment

Experimental condition			
Catalyst	n Ni/ZSM-5 (n=5, 10, and 15 wt%)	Space-time (τ) ($g_{catalyst}h/g_{WCO}$)	0.56
Temperature (°C)	700	Filling height (cm)	8
S/C	5.25	Reaction time (min)	30
Pressure (MPa)	0.1		

ment, with increased S/C, the volume fraction of H_2 and CO_2 increased, while CH_4 and CO decreased. It was finally found that H-ZSM-5 significantly increased the volume fraction of H_2 from 41.20% to 51.74%. It increased the yield of H_2 from 39.91 mol/kg to 71.47 mol/kg.

The results in Fig. 10(a) and Fig. 10(b) show that the experiment added H-ZSM-5 to produce less carbon deposition than without added H-ZSM-5. Moreover, H-ZSM-5 used in the experiment can produce more volume content of gas than without H-ZSM-5.

3-3. Effects of Content of Nickel in Catalysts on Catalyst Performance

The experimental conditions are shown in Table 6.

We determined that the optimum conditions for using H-ZSM-5 for catalytic steam reforming of WCO to produce hydrogen were 700 °C and the S/C=5.25. The work kept other conditions unchanged and we researched the effects of the content of nickel in catalysts for the experiment to produce hydrogen production of catalytic steam reforming of WCO.

As can be seen in Fig. 11, the size of the volume fraction of H_2 was: 10 wt% Ni/ZSM-5 (64.43%)>5 wt% Ni/ZSM-5 (45.61%)> 15 wt% Ni/ZSM-5 (38.36%). And the carbon deposition was as follows: 15 wt% Ni/ZSM-5 (15.38%)>10 wt% Ni/ZSM-5 (7.8%)> 5 wt% Ni/ZSM-5 (5.42%). In Fig. 9(b) and Fig. 10(a), the volume fraction of H_2 of H-ZSM-5 at 700 °C and S/C=5.25 was 51.74%, and the carbon deposition was 14.22%. The yield of H_2 at this time was 71.47 mol/kg. For the catalyst of 10 wt% Ni/ZSM-5 compared

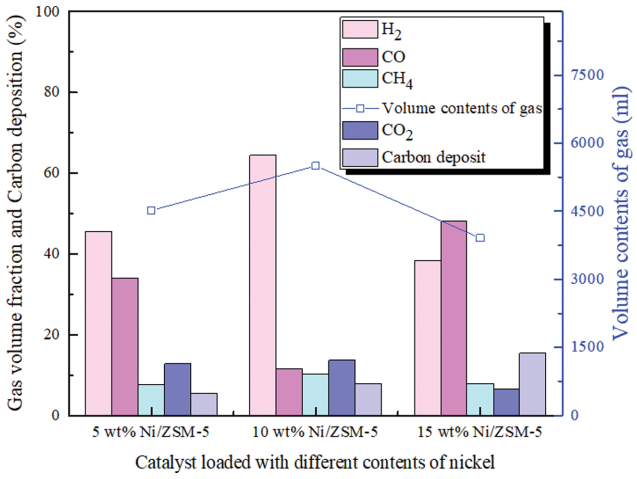

Fig. 11. Effects of gas volume fraction, carbon deposition and gas volume content on hydrogen production after using n Ni/ZSM-5 (n=5, 10, and 15 wt%) by the experiment of catalytic steam reforming of WCO.

with H-ZSM-5, the yield of H_2 increased at 55.67 mol/kg, and the carbon deposition decreased at 6.42%. Compared with H-ZSM-5, the catalyst of 5 wt% Ni/ZSM-5 reduced the yield of H_2 by 2.49 mol/kg and the carbon deposition by 8.8%. Compared with H-ZSM-5, the 15 wt% Ni/ZSM-5 decreased the yield of H_2 at 17.66 mol/kg, and the carbon deposition increased at 1.16%. In contrast, H-ZSM-5 formed more carbon deposits due to its strong acidity. The strongly acidic center promoted a series of cyclization, oligomerization, and hydrogen transfer reactions [56].

Fig. 11 displays the experimental results of three catalysts that catalyzed the steam reforming of WCO to produce hydrogen, and showed that the 10 wt% Ni/ZSM-5 catalyst could promote the cracking of WCO. The catalyst of 10 wt% Ni/ZSM-5 generated more yield of H_2 and effectively reduced the amount of carbon deposition than the other two Ni-loaded catalysts. The hydrogen yield was increased because the nickel sites on the zeolite framework facilitated the dehydrogenation reaction [47]. Moreover, the H-ZSM-5 introduced metals will enhance their catalytic activity and stability by creating metal and acid sites [44,60]. The increased Ni content promoted the $C+CO_2=2CO$ (Reaction (15)) reaction to proceed to the right, accelerated the methane reforming reaction, and enhanced the yield of H_2. The reduction of carbon deposition was due to its metal-support interaction effectively promoting the $C+H_2O=CO+H_2$ (Reaction (16)) reaction to the right. The yield of H_2 was 53.81 mol/kg, and the yield of CO was 67.59 mol/kg after the 15 wt% Ni/ZSM-5 catalyst was used in the catalytic steam reforming of WCO to produce hydrogen. Its acidity decreased when the content of nickel increased too much, so the $CO+H_2O=H_2+CO_2$ (Reaction (2)) reaction proceeded to the left. In addition, the occurrence of the carbon gasification reaction (Reaction (15)) also increased the CO content [31,61].

$$C+CO_2=2CO \quad (15)$$

$$C+H_2O=CO+H_2 \quad (16)$$

It can be seen from the comprehensive comparison of experiments that the 10 wt% Ni/ZSM-5 catalyst has a relatively good effect, which can increase the yield of hydrogen and reduce carbon deposition. However, the related carbon deposition problem is still severe. So subsequent work applied La promoted 10 wt% Ni/ZSM-5 catalyst to the experiment to further achieve high hydrogen yield and low carbon deposition during catalytic steam reforming of WCO.

3-4. Effect of Promoter (La) Addition

Because nickel is the main transition metal component in steam reforming reaction, nickel-based catalysts have attracted extensive attention for their high cost-effectiveness, good C-C and C-O bond

Table 7. Experimental conditions using 6 wt% La-10 wt% Ni/ZSM-5 in the experiment

Experimental condition			
Catalyst	6 wt% La-10 wt% Ni/ZSM-5	Space-time (τ) ($g_{catalyst}h/g_{WCO}$)	0.56
Temperature (°C)	600-800	Filling height (cm)	8
S/C	5.25	Reaction time (min)	30
Pressure (MPa)	0.1		

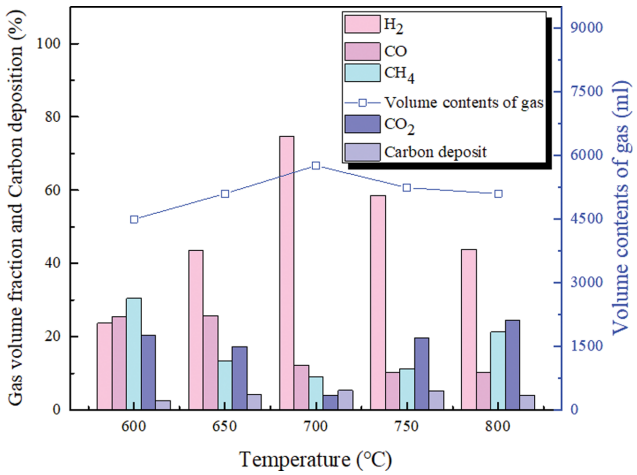

Fig. 12. The effect of 6 wt% La-10 wt% Ni/ZSM-5 catalyst on the volume fraction of gas, carbon deposition, and volume content of gas (600-800 °C).

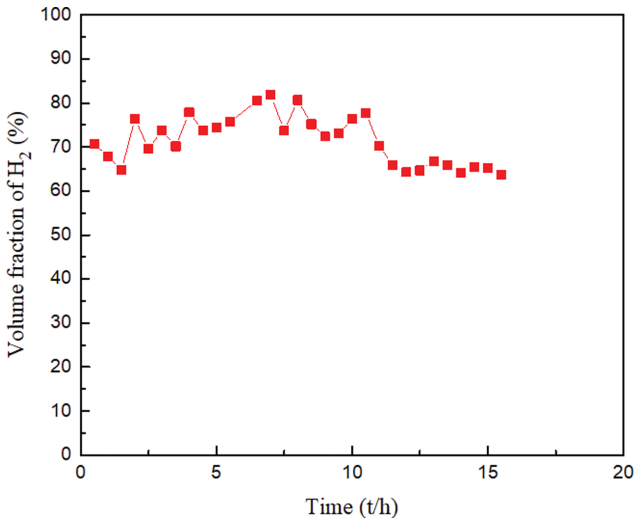

Fig. 13. Catalytic performance of 6 wt% La-10 wt% Ni/ZSM-5 for continuous reaction at 700 °C.

cracking and high thermal stability. To improve the yield of hydrogen in the catalytic steam reforming experiment of waste cooking oil, we chose nickel as the load. However, although it can promote the catalytic steam reforming experiment of waste cooking oil to improve hydrogen yield, it will also produce a carbon deposit. Introducing lanthanum (La) into the catalyst can improve the catalytic activity of the catalyst and effectively reduce carbon deposition. Moreover, the catalyst added with La can increase the alkalinity and prevent the formation of pyrolytic carbon. Therefore, lanthanum was introduced into nickel-based catalysts. The experimental conditions are shown in Table 7.

In Fig. 12, the volume fraction of H_2 first increased and decreased with the increased temperature by adding the 6 wt% La-10 wt% Ni/ZSM-5 in the experiment. The yield of H_2 was as high as 154.12 mol/kg at 700 °C, and the carbon deposit was only 5.38%. Because the steam reforming reaction $C_xH_yO_z+H_2O \xrightarrow{Catalysts} H_2+CH_4+CO+CO_2+C$ (Reaction (17)) was endothermic, so the equilibrium proceeded to the right. Furthermore, La improved the mesoporous structure and Ni dispersion of the 10 wt% Ni/ZSM-5 catalyst, which can make the $C+CO_2=2CO$ (Reaction (15)) reaction proceed to the right, and the methane reforming reaction was accelerated [62,63]. On the other hand, the steam reforming reaction $CO+H_2O=H_2+CO_2$ (Reaction (2)) and the methanation reaction $3H_2+CO=CH_4+H_2$ (Reaction (3)) were exothermic. At higher temperatures, the degree of reverse reaction of steam reforming was greater than that of the methanation reaction. Moreover, a too high temperature will lead to catalyst sintering and subsequent loss of activity, so the yield of H_2 decreased slightly after 750 °C [64].

$$C_xH_yO_z+H_2O \xrightarrow{Catalysts} H_2+CH_4+CO+CO_2+C \quad (17)$$

The Introduction of La to the catalyst can effectively promote the reaction of $C+H_2O=CO+H_2$ (Reaction (16)) to the right and reduce carbon deposition. In La-modified catalysts, since reactions (5) and (6) occurred, CO_2 adsorbed on La_2O_3 to form $La_2O_2CO_3$ intermediate, which can react with nearby carbon to generate CO to facilitate carbon removal [65,66]. Indeed, this carbon removal improvement was concurred with by Siew et al. [67], concurring with this carbon removal improvement in 2014 during their study of the effects of catalytic performance of adding La in Ni-loaded Al_2O_3 catalysts. The authors demonstrated that the alkalinity on the promoter (La) minimized the catalyst's acidity and reduced carbon deposition during the reaction [68]. Thus, the catalyst added La could increase the alkalinity and prevent the formation of pyrolytic carbon [69,70].

The results illustrated that the 6 wt% La-10 wt% Ni/ZSM-5 catalyst has a better effect on the catalytic steam reforming of WCO to produce hydrogen at 700 °C and S/C=5.25.

3-5. Stability Test of 6 wt% La-10 wt% Ni/ZSM-5

A stability test of 6 wt% La-10 wt% Ni/ZSM-5 was carried out according to the experimental conditions in Table 8. The results are shown in Fig. 13.

As shown in Fig. 13, the volume fraction of H_2 fluctuated around 76% before the reaction at 10 hours. After 10 hours, the volume fraction of H_2 began to decrease and stabilize at about 65%. Therefore, it can be concluded that the catalytic activity of 6 wt% La-10

Table 8. Experimental conditions for continuous use of 6 wt% La-10 wt% Ni/ZSM-5 catalyst

Experimental condition			
Catalyst	6 wt% La-10 wt% Ni/ZSM-5	Space-time (τ) ($g_{catalyst}h/g_{WCO}$)	0.56
Temperature (°C)	700	Filling height (cm)	8
S/C	5.25	Reaction time (h)	17
Pressure (MPa)	0.1		

wt% Ni/ZSM-5 catalyst is relatively stable.

CONCLUSION

The results in this study illustrated that the H_2 yield and anti-carbon deposition performance of the 6 wt% La-10 wt% Ni/ZSM-5 catalyst was better than the 10 wt% Ni/ZSM-5 catalyst in the experiment by catalytic reforming steam reaction of WCO. La-promoted 10 wt% Ni/ZSM-5 catalysts were suitable additives for enhancing H_2 yield and reduced the carbon deposition for hydrogen production by catalytic steam reforming of WCO, which has better catalytic properties and higher activity than bare 10 wt% Ni/ZSM-5 catalysts. As a consequence, La promoted 10 wt% Ni/ZSM-5 catalyst was applied to produce hydrogen by the experiment of catalytic steam reforming of WCO, which achieved high hydrogen yield and low carbon deposition.

ACKNOWLEDGEMENTS

The authors express their great appreciation for the financial support of this project by the National Natural Science Foundation of China (51676081), Wuhan Enterprise Technology Innovation Projects (2019020702011359; 2020020602012150), and the 111 Project B17019. Additionally, the authors would like to thank the Shiyanjia Lab (www.shiyanjia.com) for the support of SEM and NH_3-TPD tests.

REFERENCES

1. X. Dupain, D. J. Costa, C. J. Schaverien, M. Makkee and J. A. Moulijn, *Appl. Catal. B: Environ.*, **72**, 44 (2007).
2. S. Nanda, R. Rana, H. N. Hunter, Z. Fang, A. K. Dalai and J. A. Kozinski, *Chem. Eng. Sci.*, **195**, 935 (2019).
3. G. M. Allen, Dover Publications, Mineola, N.Y. (2004).
4. C. Rioche, S. Kulkarni, F. C. Meunier, J. P. Breen and R. Burch, *Appl. Catal. B: Environ.*, **61**, 130 (2005).
5. P. Fu, W. Yi, Z. Li, X. Bai, A. Zhang, Y. Li and Z. Li, *Int. J. Hydrogen Energy*, **39**, 13962 (2014).
6. H. Xie, Q. Yu, X. Yao, W. Duan, Z. Zuo and Q. Qin, *J. Energy Chem.*, **24**, 299 (2015).
7. H. D. Setiabudi, M. A. A. Aziz, S. Abdullah, L. P. Teh and R. Jusoh, *Int. J. Hydrogen Energy*, **45**, 18376 (2020).
8. C. G. Vayenas, *J. Catal.*, **134**, 755 (1992).
9. I. N. Buffoni, F. Pompeo, G. F. Santori and N. N. Nichio, *Catal. Commun.*, **10**, 1656 (2009).
10. N. Goyal, K. K. Pant and R. Gupta, *Int. J. Hydrogen Energy*, **38**, 921 (2013).
11. J. Chen, J. Sun and Y. Wang, *Ind. Eng. Chem. Res.*, **56**, 4627 (2017).
12. B. Yan, W. Li, J. Tao, N. Xu, X. Li and G. Chen, *Int. J. Hydrogen Energy*, **42**, 6674 (2017).
13. A. Awadallah, A. Aboul-Enein and A. Aboul-Gheit, *Renew. Energy*, **57**, 671 (2013).
14. N. Gutta, V. K. Velisoju, A. Chatla, V. Boosa, J. Tardio, J. Patel and V. Akula, *Energy Fuels*, **32**, 4008 (2018).
15. X. Zhao, K. Wu, W. Liao, Y. Wang, X. Hou, M. Jin, Z. Suo and H. Ge, *Green Energy Environ.*, **4**, 300 (2019).
16. S. Zhou, Z. Chen, H. Gong, X. Wang, T. Zhu and Y. Zhou, *Appl. Catal. A: Gen.*, **607**, 117859 (2020).
17. R. S. Tan, T. A. Tuan Abdullah, A. Ripin, A. Ahmad and K. Md Isa, *J. Environ. Chem. Eng.*, **7**, 103490 (2019).
18. X. Li, D. Li, H. Tian, L. Zeng, Z.-J. Zhao and J. Gong, *Appl. Catal. B: Environ.*, **202**, 683 (2017).
19. S. Adamu, H. Binous, S. A. Razzak and M. M. Hossain, *Renew. Energy*, **111**, 399 (2017).
20. M. B. I. Chowdhury, M. Z. Hossain, J. Mazumder, A. K. Jhawar and P. A. Charpentier, *Fuel*, **217**, 166 (2018).
21. M. Boudjeloud, A. Boulahouache, C. Rabia and N. Salhi, *Int. J. Hydrogen Energy*, **44**, 9906 (2019).
22. H. Lu, X. Yang, G. Gao, J. Wang, C. Han, X. Liang, C. Li, Y. Li, W. Zhang and X. Chen, *Fuel*, **183**, 335 (2016).
23. A. A. Abdulrasheed, A. A. Jalil, M. Y. S. Hamid, T. J. Siang and T. A. T. Abdullah, *J. CO_2 Util.*, **37**, 230 (2020).
24. P. Osorio-Vargas, N. A. Flores-González, R. M. Navarro, J. L. G. Fierro, C. H. Campos and P. Reyes, *Catal. Today*, **259**, 27 (2016).
25. E. Kok, J. Scott, N. Cant and D. Trimm, *Catal. Today*, **164**, 297 (2011).
26. M. Chen, X. Li, Y. Wang, C. Wang, T. Liang, H. Zhang, Z. Yang, Z. Zhou and J. Wang, *Energy Conv. Manage.*, **184**, 315 (2019).
27. Z. Li, Z. Zhong, B. Zhang, W. Wang and W. Wu, *J. Anal. Appl. Pyrolysis*, **138**, 103 (2019).
28. Y. Li, Nishu, D. Yellezuome, M. Chai, C. Li and R. Liu, *J. Energy Inst.*, **99**, 218 (2021).
29. Y. Wang, C. Wang, M. Chen, J. Hu, Z. Tang, D. Liang, W. Cheng, Z. Yang, J. Wang and H. Zhang, *Fuel*, **279**, 118449 (2020).
30. M. Chen, D. Liang, Y. Wang, C. Wang, Z. Tang, C. Li, J. Hu, W. Cheng, Z. Yang, H. Zhang and J. Wang, *Int. J. Hydrogen Energy*, **46**, 21796 (2021).
31. Nishu, C. Li, M. Chai, M. M. Rahman, Y. Li, M. Sarker and R. Liu, *Renew. Energy*, **175**, 936 (2021).
32. S. S. Vieira, Z. M. Magriotis, I. Graça, A. Fernandes, M. F. Ribeiro, J. M. F. M. Lopes, S. M. Coelho, N. A. V. Santos and A. A. Saczk, *Catal. Today*, **279**, 267 (2017).
33. R. Yang, C. Xing, C. Lv, L. Shi and N. Tsubaki, *Appl. Catal.s A: Gen.*, **385**, 92 (2010).
34. H. Su, E. Kanchanatip, D. Wang, H. Zhang, Antoni, I. Mubeen, Z.

Huang and M. Yan, *Int. J. Hydrogen Energy*, **45**, 553 (2020).
35. H. Lorenz, S. Turner, O. I. Lebedev, G. Van Tendeloo, B. Klötzer, C. Rameshan, K. Pfaller and S. Penner, *Appl. Catal. A: Gen.*, **374**, 180 (2010).
36. Z. Li, X. Yang, Y. Han and L. Rong, *Int. J. Hydrogen Energy*, **45**, 21364 (2020).
37. L. N. Jun, M. B. Bahari, H. D. Setiabudi, A. A. Jalil and D.-V. N. Vo, *Process Saf. Environ. Prot.*, **150**, 356 (2021).
38. T. Pan, S. Ge, M. Yu, Y. Ju, R. Zhang, P. Wu, K. Zhou and Z. Wu, *Fuel*, **311**, 122629 (2022).
39. Y. Zheng, F. Wang, X. Yang, Y. Huang, C. Liu, Z. Zheng and J. Gu, *J. Anal. Appl. Pyrolysis*, **126**, 169 (2017).
40. J. Zhang, M. Ren, X. Li, Q. Hao, H. Chen and X. Ma, *Energy Conv. Manage.*, **205**, 112419 (2020).
41. S. S. Miri, F. Meshkani, A. Rastegarpanah and M. Rezaei, *Chem. Eng. Sci.*, **250**, 116956 (2022).
42. T. A. Le, Q. C. Do, Y. Kim, T.-W. Kim and H.-J. Chae, *Korean J. Chem. Eng.*, **38**, 1087 (2021).
43. Z. Hao, Q. Zhu, Z. Jiang, B. Hou and H. Li, *Fuel Process. Technol.*, **90**, 113 (2009).
44. A. Kostyniuk, D. Bajec and B. Likozar, *Renew. Energy*, **167**, 409 (2021).
45. P. Feng, K. Huang, Q. Xu, W. Qi, S. Xin, T. Wei, L. Liao and Y. Yan, *Int. J. Hydrogen Energy*, **45**, 8223 (2020).
46. L. Chen, H. Li, J. Fu, C. Miao, P. Lv and Z. Yuan, *Catal. Today*, **259**, 266 (2016).
47. S. Pinjari, M. K. Kumaravelan, V. C. Peddy, S. Gandham, J. Patruni, S. Velluru and P. Kumar, *Int. J. Hydrogen Energy*, **43**, 2781 (2018).
48. R. Tian, S.-y. Wang, C.-s. Lian, X. Wu, X. An and X.-m. Xie, *J. Fuel Chem. Technol.*, **47**, 1476 (2019).
49. Z. Niazi, A. Irankhah, Y. Wang and H. Arandiyan, *Int. J. Hydrogen Energy*, **45**, 21512 (2020).
50. Y. Sugi, Y. Kubota, K. Komura, N. Sugiyama, M. Hayashi, J. H. Kim and G. Seo, *Appl. Catal. A: Gen.*, **299**, 157 (2006).
51. K. Ding, A. He, D. Zhong, L. Fan, S. Liu, Y. Wang, Y. Liu, P. Chen, H. Lei and R. Ruan, *Bioresour. Technol.*, **268**, 1 (2018).
52. M. Li, S. Xing, L. Yang, J. Fu, P. Lv, Z. Wang and Z. Yuan, *Appl. Catal. A: Gen.*, **587**, 117112 (2019).
53. X. Zhang, H. Lei, G. Yadavalli, L. Zhu, Y. Wei and Y. Liu, *Fuel*, **144**, 33 (2015).
54. X. Li, B. Li, J. Xu, Q. Wang, X. Pang, X. Gao, Z. Zhou and J. Piao, *Appl. Clay Sci.*, **50**, 81 (2010).
55. L. Fan, R. Ruan, J. Li, L. Ma, C. Wang and W. Zhou, *Appl. Energy*, **263**, 114629 (2020).
56. F. Li, S. Ding, Z. Wang, Z. Li, L. Li, C. Gao, Z. Zhong, H. Lin and C. Chen, *Energy Fuels*, **32**, 5910 (2018).
57. J. Xu and G. F. Froment, *AIChE J.*, **35**, 88 (1989).
58. N. Kaisalo, P. Simell and J. Lehtonen, *Fuel*, **182**, 696 (2016).
59. M. Koike, D. Li, H. Watanabe, Y. Nakagawa and K. Tomishige, *Appl. Catal. A: Gen.*, **506**, 151 (2015).
60. S. C. Srivatsa, F. Li and S. Bhattacharya, *Renew. Energy*, **142**, 426 (2019).
61. G.-Q. Wei, W.-N. Zhao, J.-G. Meng, J. Feng, W.-Y. Li, F. He, Z. Huang, Q. Yi, Z.-Y. Du, K. Zhao, Z.-L. Zhao and H.-B. Li, *J. Clean. Prod.*, **200**, 588 (2018).
62. L. Qian, Z. Ma, Y. Ren, H. Shi, B. Yue, S. Feng, J. Shen and S. Xie, *Fuel*, **122**, 47 (2014).
63. H. Su, E. Kanchanatip, D. Wang, H. Zhang, Antoni, I. Mubeen, Z. Huang and M. Yan, *Int. J. Hydrogen Energy*, **45**, 553 (2020).
64. W. Liu and H. Yuan, *Int. J. Energy Res.*, **44**, 11564 (2020).
65. F. Fayaz, B. Long Giang, M. B. Bahari, N. Trinh Duy, B. V. Khanh, R. Kanthasamy, C. Samart, N.-H. Chinh and D.-V. N. Vo, *Int. J. Energy Res.*, **43**, 405 (2019).
66. K.-H. Lin, C.-B. Wang and S.-H. Chien, *Int. J. Hydrogen Energy*, **38**, 3226 (2013).
67. K. W. Siew, H. C. Lee, J. Gimbun and C. K. Cheng, *Int. J. Hydrogen Energy*, **39**, 6927 (2014).
68. L. N. Jun, M. B. Bahari, H. D. Setiabudi, A. A. Jalil and D.-V. N. Vo, *Process Saf. Environ. Prot.*, **150**, 356 (2021).
69. T. Bai, X. Zhang, F. Wang, W. Qu, X. Liu and C. Duan, *J. Energy Chem.*, **25**, 545 (2016).
70. Y. Ni, A. Sun, X. Wu, G. Hai, J. Hu, T. Li and G. Li, *J. Colloid Interface Sci.*, **361**, 521 (2011).